Numerical Simulation of Flow Around a Three-Dimensional Turret

S. C. Purohit*
University of Dayton Research Institute, Dayton, Ohio
and
J. S. Shang† and W. L. Hankey Jr.‡
Air Force Wright Aeronautical Laboratories, Wright-Patterson Air Force Base, Ohio

The compressible Navier-Stokes equations in mass averaged variables are numerically solved for flow around a surface mounted turret. The three-dimensional unsteady separated flow is investigated with emphasis on the near wake region. The computation is performed on the CRAY-1 computer using MacCormack's explicit finite difference scheme. For the freestream Mach number 0.55 and Reynolds number 10.3×10^6/m, the time-dependent calculation is carried out for 55,800 grid points in the computational domain to achieve steady-state periodic solution. The entire flowfield around the turret is analyzed and comparison with available experimental data is reported.

Nomenclature

AZA	= azimuth angle around turret
CP	= pressure coefficient
D	= turret diameter
ds_1, ds_2	= arc lengths
e	= specific energy
e_i	= specific internal energy, $C_v \cdot T$
F,G,H	= vector fluxes in mean flow equations
J	= Jacobian of coordinate transformation
N,N'	= singular point, node
P	= pressure
Pr	= molecular Prandtl number, 0.72
Pr_t	= turbulent Prandtl number, 0.90
R	= turret radius
S,S'	= singular point, saddle point
t	= time
T	= temperature
T_{ch}	= characteristic time, D/U_∞
u,v,w	= velocity components in Cartesian coordinates
U	= mass-averaged dependent variable
U_{max}	= maximum velocity in near wake
x,y,z	= Cartesian coordinates
ρ	= density
ξ,η,ζ	= transformed coordinates
ϵ	= eddy viscosity
γ	= ratio of specific heats
μ	= molecular viscosity coefficient
δ_i^*	= kinematic displacement
ω	= vorticity
Σ	= summation

Subscripts

∞	= freestream condition
w	= surface condition

Introduction

THE understanding and analysis of three-dimensional fluid behavior around a surface mounted blunt obstacle (turret) is of considerable importance for flight applications. The prime motivation to solve such problems is to investigate the basic phenomenon of separated flow and to determine the associated forces on the object. In addition, the dynamic features of the unsteady flowfield around the obstacle are of interest to the designer.

The time variation of the separation line due to the shedding of vortices for the flow past a turret produces a complex and intriguing flow structure. Also, the appropriate turbulence model, ranges of Mach number and Reynolds number, and protuberance height are some of the elements in parametric space which restrict the unified approach and generality of the solution. The experimental and computational approaches are the common aerodynamic tools to investigate complex problems. However, during recent years, the computational approach has been preferred because of its lower cost, the availability of faster computers, and detailed description of the fluid physics. In this frame of reference, the present work addresses the "computational flow visualization" of the three-dimensional separated flow. The primary objectives are to provide an efficient numerical procedure for the solution of the governing equations and to compare the computed results with the previously obtained experimental data.

The experimental results[1-5] obtained primarily by conventional flow visualization techniques and the data correlated indicate some important facts about the primary separation features for flow past small protuberances. For different protuberance heights, the available flowfield data is so sparse that its interpretation leading to a general conclusion is not obvious. To acquire the finer details, it is felt that the three-dimensional separated flow past a turret requires numerical analysis.

Influenced by the results of experimental studies for a proper criterion for three-dimensional flow separation led to a simple convincing topological approach.[6-9] This approach is based on the hypothesis that vector fields of the skin friction lines and external streamlines remain continuous. Taking bodies of revolution at various angles of incidence, for example, it was possible to synthesize the flow mechanism in a rational manner. We will be using some of these topological ideas to exaplain the fluid behavior around the turret.

Turning to our present effort, for subsonic high Reynolds number flow, past a hemispherically capped cylindrical obstacle (the turret), the horseshoe vortex, turbulent boundary-layer characteristics, and near wake structure need careful attention, particularly from a numerical simulation point of view. A subset of this immense problem, unsteady flow

Presented as Paper 82-1020 at the AIAA/ASME Third Joint Thermophysics, Fluids, Plasma and Heat Transfer Conference, St. Louis, Mo., June 7-11, 1982; submitted June 17, 1982; revision received Dec. 6, 1982. This paper is declared a work of the U.S. Government and therefore is in the public domain.

*Visiting Scientist, Aerospace Mechanics Division. Member AIAA.
†Aerospace Engineer. Associate Fellow AIAA.
‡Technical Manager. Associate Fellow AIAA.

oscillations past a circular cylinder, was recently studied by Shang.[10] In that numerical experiment, the mesh point distribution and appropriate boundary conditions were optimized to yield the time mean and fluctuating properties of the fluid. This two-dimensional computation provided encouragement to continue further and analyze the large-scale organized fluid motion around a three-dimensional turret at a Mach number of 0.55 and a Reynolds number of 10.3×10^6/m. At these conditions the turret height is much larger than that of the turbulent boundary layer on the surface. The aim is to evaluate the density field and its fluctuations around the turret and compare the results with the experimental data.[11]

Analysis

For the problem under consideration, the solution of unsteady compressible Navier-Stokes equations becomes necessary. These equations offer, on a fine scale, a good insight into the viscous-inviscid interaction and the separated flow structure. For the present Reynolds number range, the flow along the flat plate as well as around the turret will be turbulent and, thus, adequate inclusion of turbulence terms is needed. Using body-oriented coordinate transformation, in the absence of body forces and electromagnetic effects, the Navier-Stokes equations, in mass-averaged variables, can be written in the following convenient form:

$$\frac{\partial U}{\partial t}+\begin{bmatrix}\xi_x\\ \xi_y\\ \xi_z\end{bmatrix}\left(\frac{\partial F}{\partial\xi},\frac{\partial G}{\partial\xi},\frac{\partial H}{\partial\xi}\right)+\begin{bmatrix}\eta_x\\ \eta_y\\ \eta_z\end{bmatrix}\left(\frac{\partial F}{\partial\eta},\frac{\partial G}{\partial\eta},\frac{\partial H}{\partial\eta}\right)+\begin{bmatrix}\zeta_x\\ \zeta_y\\ \zeta_z\end{bmatrix}\left(\frac{\partial F}{\partial\zeta},\frac{\partial G}{\partial\zeta},\frac{\partial H}{\partial\zeta}\right)=0 \tag{1}$$

where

$$U=\begin{bmatrix}\rho\\ \rho u\\ \rho v\\ \rho w\\ \rho e\end{bmatrix} \tag{2}$$

$$F=\begin{bmatrix}\rho u\\ \rho u^2+\sigma_x\\ \rho uv+\tau_{xy}\\ \rho uw+\tau_{xz}\\ (\rho e+\sigma_x)u+\tau_{xy}\cdot v+\tau_{xz}\cdot w-\dot q_x\end{bmatrix} \tag{3}$$

$$G=\begin{bmatrix}\rho v\\ \rho vu+\tau_{yx}\\ \rho v^2+\sigma_y\\ \rho vw+\tau_{yz}\\ (\rho e+\sigma_y)v+\tau_{yx}\cdot u+\tau_{yz}\cdot w-\dot q_y\end{bmatrix} \tag{4}$$

$$H=\begin{bmatrix}\rho w\\ \rho wu+\tau_{zx}\\ \rho wv+\tau_{zy}\\ \rho w^2+\sigma_z\\ (\rho e+\sigma_z)w+\tau_{zx}\cdot u+\tau_{zy}\cdot v-\dot q_z\end{bmatrix} \tag{5}$$

$$\sigma_x=p+\frac{2}{3}(\mu+\epsilon)\left(\frac{\partial u}{\partial x}+\frac{\partial v}{\partial y}+\frac{\partial w}{\partial z}\right)-2(\mu+\epsilon)\frac{\partial u}{\partial x} \tag{6a}$$

$$\tau_{xy}=\tau_{yx}=-(\mu+\epsilon)\left(\frac{\partial u}{\partial y}+\frac{\partial v}{\partial x}\right) \tag{6b}$$

$$\tau_{xz}=\tau_{zx}=-(\mu+\epsilon)\left(\frac{\partial u}{\partial z}+\frac{\partial w}{\partial x}\right) \tag{6c}$$

$$\sigma_y=p+\frac{2}{3}(\mu+\epsilon)\left(\frac{\partial u}{\partial x}+\frac{\partial v}{\partial y}+\frac{\partial w}{\partial z}\right)-2(\mu+\epsilon)\frac{\partial v}{\partial y} \tag{6d}$$

$$\tau_{yz}=\tau_{zy}=-(\mu+\epsilon)\left(\frac{\partial v}{\partial z}+\frac{\partial w}{\partial y}\right) \tag{6e}$$

$$\sigma_z=p+\frac{2}{3}(\mu+\epsilon)\left(\frac{\partial u}{\partial x}+\frac{\partial v}{\partial y}+\frac{\partial w}{\partial z}\right)-2(\mu+\epsilon)\frac{\partial w}{\partial z} \tag{6f}$$

$$\dot q_x=\gamma\left(\frac{\mu}{Pr}+\frac{\epsilon}{Pr_t}\right)\frac{\partial e_i}{\partial x} \tag{7a}$$

$$\dot q_y=\gamma\left(\frac{\mu}{Pr}+\frac{\epsilon}{Pr_t}\right)\frac{\partial e_i}{\partial y} \tag{7b}$$

$$\dot q_z=\gamma\left(\frac{\mu}{Pr}+\frac{\epsilon}{Pr_t}\right)\frac{\partial e_i}{\partial z} \tag{7c}$$

$$e=e_i+(u^2+v^2+w^2)/2.0 \tag{8}$$

This system of equations is closed by a perfect gas law, Sutherland's viscosity formula, and an appropriate eddy viscosity model as a supplementary relation.

The fluid motion defined by the aforementioned set of equations is to be analyzed around a turret (Fig. 1) mounted on a flat surface. Its base is a circular cylinder with a diameter of 0.44 m and a height to diameter ratio of 1.071. One of the sides has a cut-out (window) at a normal distance 0.194 m from the turret axis. The top of the turret is a hemispherical dome of radius 0.223 m whose center is on the axis. The ξ,η,ζ correspond to axial, normal, tangential transformed coordinates of the turret, respectively. The origin of the coordinates is located at the intersection of the turret axis and the

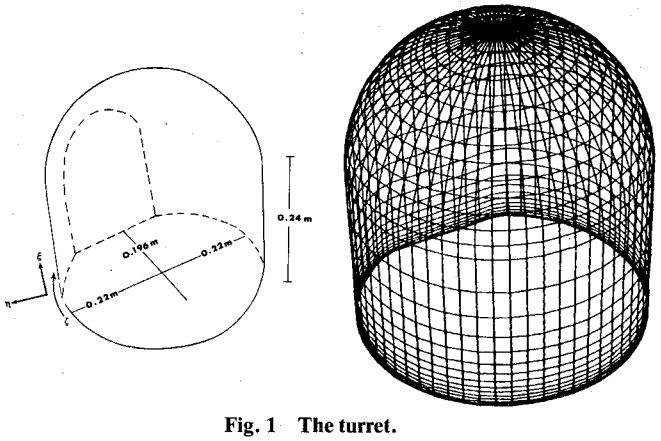

Fig. 1 The turret.

flat surface. For this configuration, the experimental results[11] were available for various locations of the turret window (look angle). In order to demonstrate, a typical flowfield for a 90-deg look angle was simulated. The (azimuth) angle is measured clockwise from the oncoming freestream direction.

One of the major tasks in numerical simulation is the proper selection of mesh system in the computational domain. A judicious choice of grid points helps capture the important flowfield characteristics as well as reducing the data processing time. After much study the following choice was made. The turret surface is defined by 62×30 points. On the cylindrical portion, 15 points were used in the axial direction stretched exponentially from the base and 15 points were uniformly placed on the hemispherical dome. In the tangential direction 62 equidistant points were used with first and last two overlapping points to permit the use of fourth-order pressure damping. Using these surface nodes as the reference points, the normal coordinates are then described by 30 exponentially stretched points from the turret surface extending outward to ten times the turret radius. The finer mesh near the turret and flat plate will help resolve the viscous effects while the coarser mesh helps reduce the computational time. Care has been taken that no mesh point lies on the turret axis. This precaution makes the Jacobian of the coordinate transformation $J=\partial(\xi,\eta,\zeta)/\partial(x,y,z)$, a nonsingular determinant and allows a one-to-one correspondence from the physical to the transformed space.

The well-posed and stable boundary conditions for subsonic Navier-Stokes equations are still uncertain. However, for three-dimensional flows the disturbances generated by the turret decay rapidly. If the boundary conditions are specified at a sufficiently large distance away from the turret, the over-specification is generally acceptable. Initially, the turret is assumed to be immersed completely in the uniform stream. The upstream boundary conditions are the freestream values, whereas at the downstream side the gradient of the properties is assumed to vanish. On the solid surfaces, the no-slip conditions for the velocity components, along with a prescribed wall temperature, are imposed; while near the turret axis, an interpolation is adopted to eliminate calculation on this singularity. Along the coinciding planes (azimuth angles 0 and 360 deg), the conditions were numerically matched at all the mesh points. Thus, the following conditions are applied on the unit cube (Fig. 2) in the transformed plane $0\le\xi,\eta,\zeta\le1$.

Initial conditions

$$U(0,\xi,\eta,\zeta)=U_\infty \tag{9}$$

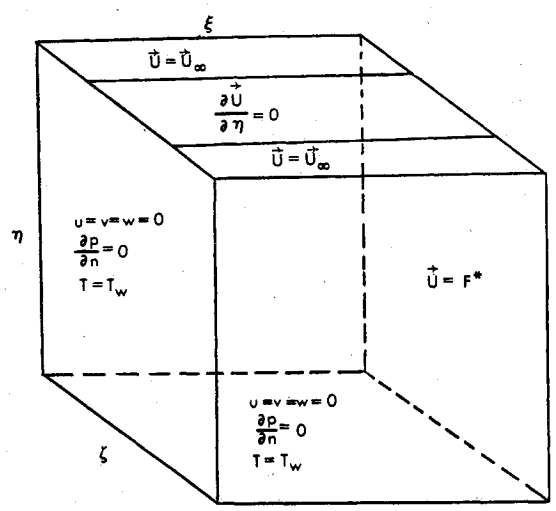

Fig. 2 Boundary conditions (transformed space).

Boundary conditions

Upstream:

$$U(t,\xi,1,\zeta_0)=U_\infty, \qquad \zeta_0<\zeta_2, \quad \zeta_0>\zeta_1 \tag{10}$$

where ζ_0 is a particular value of ζ corresponding to all the grid points facing the upcoming flow (ζ_2 for the azimuth angle 90 deg and ζ_1 for the azimuth angle 270 deg).

Downstream:

$$\frac{\partial}{\partial\eta}U(t,\xi,\eta,\zeta)\,|_{\eta=1}=0 \tag{11}$$

On the solid surfaces:

$$u=v=w=0 \tag{12a}$$

$$T_w=1.0584\cdot T_\infty \tag{12b}$$

$$\partial P/\partial n=0 \tag{12c}$$

where n is the direction normal to the surface.

Near the turret axis:

$$U(t,1,\eta,\zeta)=F^* \tag{13}$$

where

$$F^*=\frac{ds_2}{2(ds_1+ds_2)}\cdot U(t,1-\Delta\xi,\eta,\zeta+30\Delta\zeta)$$

$$+\frac{ds_2+2ds_1}{2(ds_1+ds_2)}U(t,1-\Delta\xi,\eta,\zeta)$$

It may be recalled that there are 60 equidistant mesh points in the tangential direction and $\zeta+30\Delta\zeta$ will identify the diagonally opposite mesh point across the turret axis. The terms ds_1 and ds_2 are the arc lengths subtended by the mesh points $(1,\eta,\zeta)$ and $(1-\Delta\xi,\eta,\zeta)$ along the turret axis to the center of the hemisphere (turret top).

Eddy Viscosity Model

The closure of the system of equations is achieved by using a Cebeci-Smith type eddy viscosity model and by assigning a turbulent Prandtl number of 0.90.

In the inner region:

$$\epsilon_i=\rho(K_1LD_1)^2\,|\omega| \tag{14}$$

where ω is the vorticity of the flowfield. In the present formulation, the Van Driest's damping factor is given as

$$D_1=1-\exp\left(-\sqrt{\frac{\rho_w\,|\omega_w|}{\mu_w}}L/25\right) \tag{15}$$

and the scaling length L is the distance measured along the outward normal from the turret surface.

In the downstream wake region, we use the modified Clauser's law,

$$\xi_0=0.00168\rho_\infty U_{\max}\delta_i^* \tag{16}$$

where δ_i^* is the kinematic displacement thickness of the wake in the plane of turret shoulder (the intersection of hemisphere and the cylinder). This thickness is evaluated at a downstream distance about six times the turret radius.

$$\delta_i^* = \int_{\zeta_1}^{\zeta_2} \left(1 - \frac{u^2+v^2+w^2}{U_{\max}^2}\right) d\zeta$$

Thus instantaneous effective eddy viscosity is taken to be

$$\epsilon = \min(\epsilon_0, \epsilon_i) \tag{17}$$

Numerical Procedure

The present investigation utilizes the well-established vector solver[12,13] which adopts, basically, the MacCormack's explicit finite difference scheme.[14] Owing to the large memory availability and high data processing rate (the CPU time per grid point per time iteration), the computer CRAY-1 was used for our computation. The intricate interplay between its capacity and numerical scheme provided an efficient and powerful tool to analyze this three-dimensional problem with acceptable engineering accuracy.

We used the solver to initialize the planes or "pages" in the (η-ζ) plane and to sweep, for each time step, in the ξ direction, thus minimizing the data flow from and to the disk or mass storage devices. The vector length for this case was 62 which is also the longest index array of the three-dimensional mesh system. The computational facilities were utilized with remote access via long distance dial up and the SAMNET network link. The data processing rate of 6.8×10^{-5} s was achieved for the present analysis. Most of the available memory was required to perform the time-dependent calculations.

The finer mesh sizes in the normal direction of the turret and flat surface were 0.357×10^{-2} m and 0.345×10^{-2} m, respectively, whereas the coarser mesh sizes were 0.831×10^{-1} m, and the angular displacement between nodes was 6 deg. These mesh sizes seem to provide satisfactory time-step increments during the computation. Further refinement could result in the stiffened behavior of the transformation metric element near the dome and/or much smaller time step. A conservative choice of the Courant-Fredrich-Lewy (CFL = 0.6) condition was implemented to have optimum time step with stable numerical evolution.

Once the initial phase of computation was completed and some anticipated periodicity in the flow characteristics was observed, the evaluation of the root mean square (rms) density fluctuation was attempted. For turbulent compressible flow, separating the time mean and fluctuations of density, the squared density fluctuation over a characteristic time period was calculated as

$$\langle \rho'^2 \rangle = \frac{1}{T_p} \int_t^{t+T_p} \rho^2 dt - \left[\frac{1}{T_p} \int_t^{t+T_p} \rho dt\right]^2 \tag{18}$$

where T_p is the principal time period, equal to 0.0114 s and is a function of Strouhal number, turret diameter, and freestream velocity. The computation of rms density for all grid points required three times the additional available computer memory, which is not feasible at this stage. Therefore, this particular analysis was confined to a part of the computational domain from a turret height $Y/R = 0.4$ to $Y/R = 1.7$. A total of 2.7 h CPU time of CRAY-1 computer were required to calculate the entire flow and the rms density fluctuations over one principal period. For this computation, the maximum memory used was 800K decimal words which was close to the available CRAY-1 memory.

Results and Discussions

We divide this section into two main categories. The first of these will deal with the comparison of the computed and experimental results.[11] This permits the validation of our computational procedure as well as providing guidelines for the subsequent analysis. The rest of the discussion is concentrated on probing into the different aspects of three-dimensional separated flow structures.

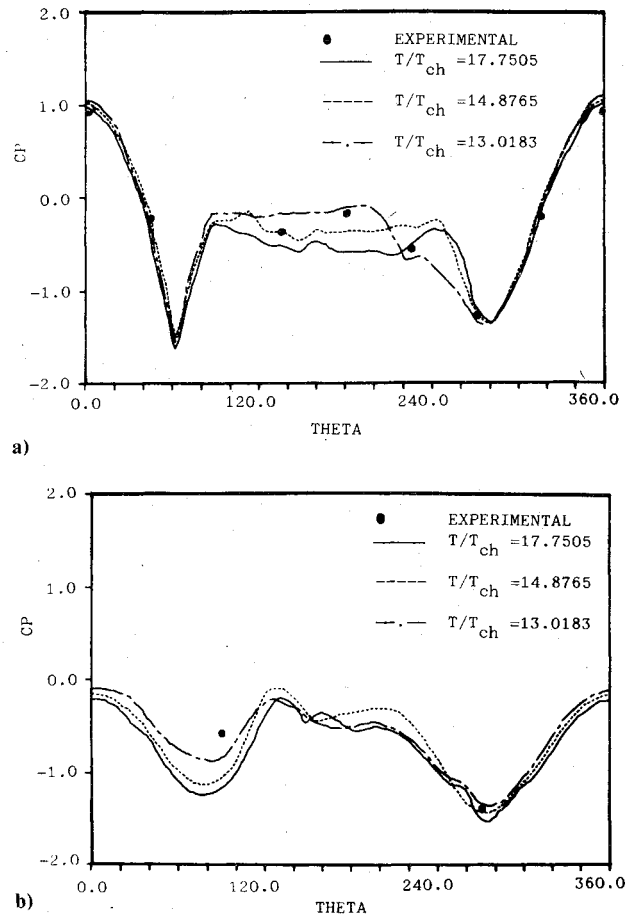

Fig. 3 Comparison of *CP* distribution, a) at the turret surface and b) on the hemispherical surface, 45 deg MPA.

The pressure coefficient distribution at the turret shoulder and 45 deg meridian plane angle (MPA) are presented in Fig. 3. The variable theta is the azimuth angle measured clockwise from the oncoming freestream direction. Thus, the cut-out side of the turret is located in the range 0-180 deg and the smooth side is between 180 and 360 deg. We will adhere to the same definition throughout our discussion. The comparison shows good agreement with the experimental results. The different curves represent the variation in pressure coefficient during one principal time period. At the turret shoulder, where the cylindrical and hemispherical surfaces meet, the computed mean *CP* (Fig. 3a) is 0.9918 for the forward stagnation point (AZA = 0 deg) whereas the measured value is 0.91. The front edge of the turret window experiences a sudden expansion of the flow and a small separation zone resulting in a steep drop in pressure (AZA = 63 deg) and a rapid pressure recovery within 20 deg in the downstream direction. The smooth side does not witness such abrupt changes and gives way to minimum pressure value at AZA = 279 deg. For a 45 deg MPA, on the hemispherical surface, (Fig. 3b), the *CP* distribution exhibits relatively smooth variation. It also hints that the presence of the turret window has very small effects for this meridian plane (45 deg MPA).

This argument is further confirmed by Fig. 4, which shows the instantaneous pressure coefficient contours of different levels around the turret surface. A zone of very low pressure can be observed at the turret window spread over 10 deg azimuth angles extending from slightly above the flat surface on to the hemisphere up to 37 deg MPA. The low valued pressure contours are mostly confined to the rear side of the turret for azimuth angles of 80-300 deg. At the turret top, the averaged computed value is -1.27 which is lower than the experimental value -1.0. It may be recalled that the turret

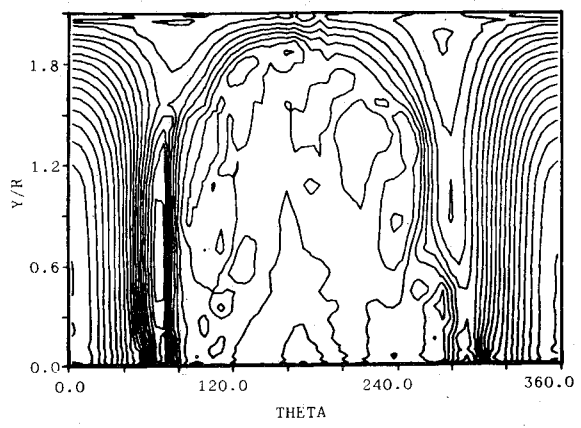

Fig. 4 Instantaneous *CP* distribution contours around the turret.

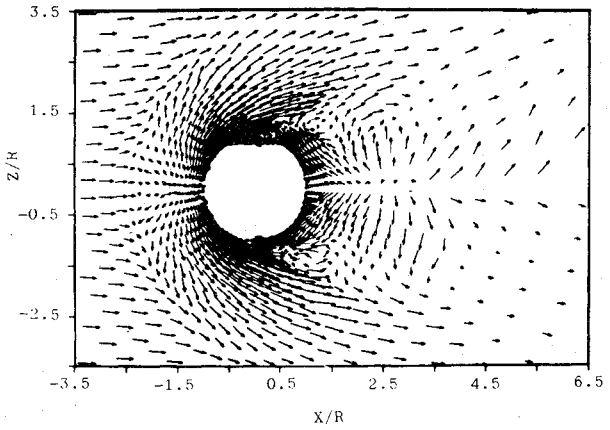

Fig. 5 Limiting streamline pattern on the flat surface.

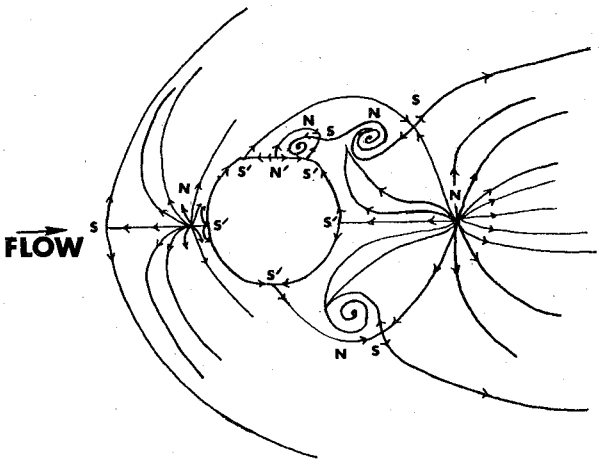

Fig. 6 Interpretation of the skin friction lines on the flat surface.

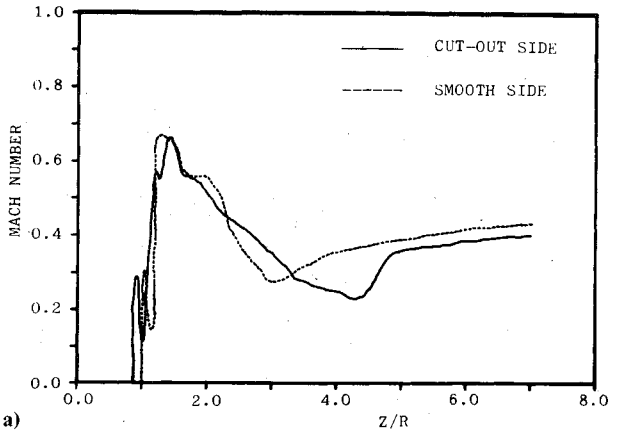

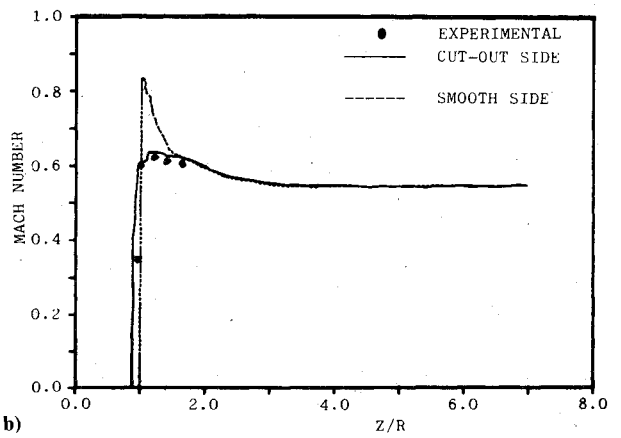

Fig. 7 Mach number distribution, a) close to the flat surface and b) at the turret shoulder.

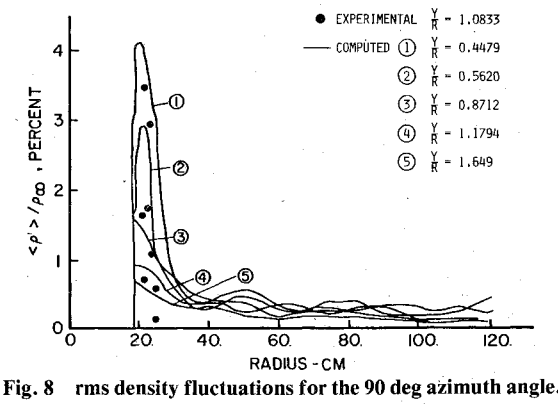

Fig. 8 rms density fluctuations for the 90 deg azimuth angle.

top is in the vicinity of 60 clustered mesh points, none of which is at the top. Our pressure coefficient value is the mean of the values at all these points. This difference may be attributed to the grid point arrangement and the improvement in this direction is one of our future goals.

A significant insight into the separated flow is offered by the limiting streamline pattern, which is, in the limiting case, the skin friction lines on the flat surface around the turret. In Fig. 5, we present a typical development of such lines that agrees qualitatively to the work of Sedney and Kitchens.[1] The primary separation line located at twice the turret radius upstream of the forward stagnation point and the atachment lines are quite clear and distinct. However, the secondary separation appears on and off near the primary separation line, very close to the plane of symmetry, indicating that it lifts off the surface very quickly. The observation will be further confirmed when we discuss the flowfield in the cross-sectional plane. The primary separation line that encircles the turret front and extends downstream in the asymmetric plane, finally becomes a leg of the horseshoe vortex.

The asymmetry in the plane induced by the turret window contains some spectacular features in the downstream direction. The vortical motion in the near wake is produced by the adverse pressure gradient at the separation points and near turret window edge. This characteristic behavior gives rise to the number of singular points. The detailed information regarding these points is shown in Fig. 6. The consistency in the fluid motion can be further confirmed by catagorizing the singular points (Hut et al.[7]): N=(number of nodes)=5,

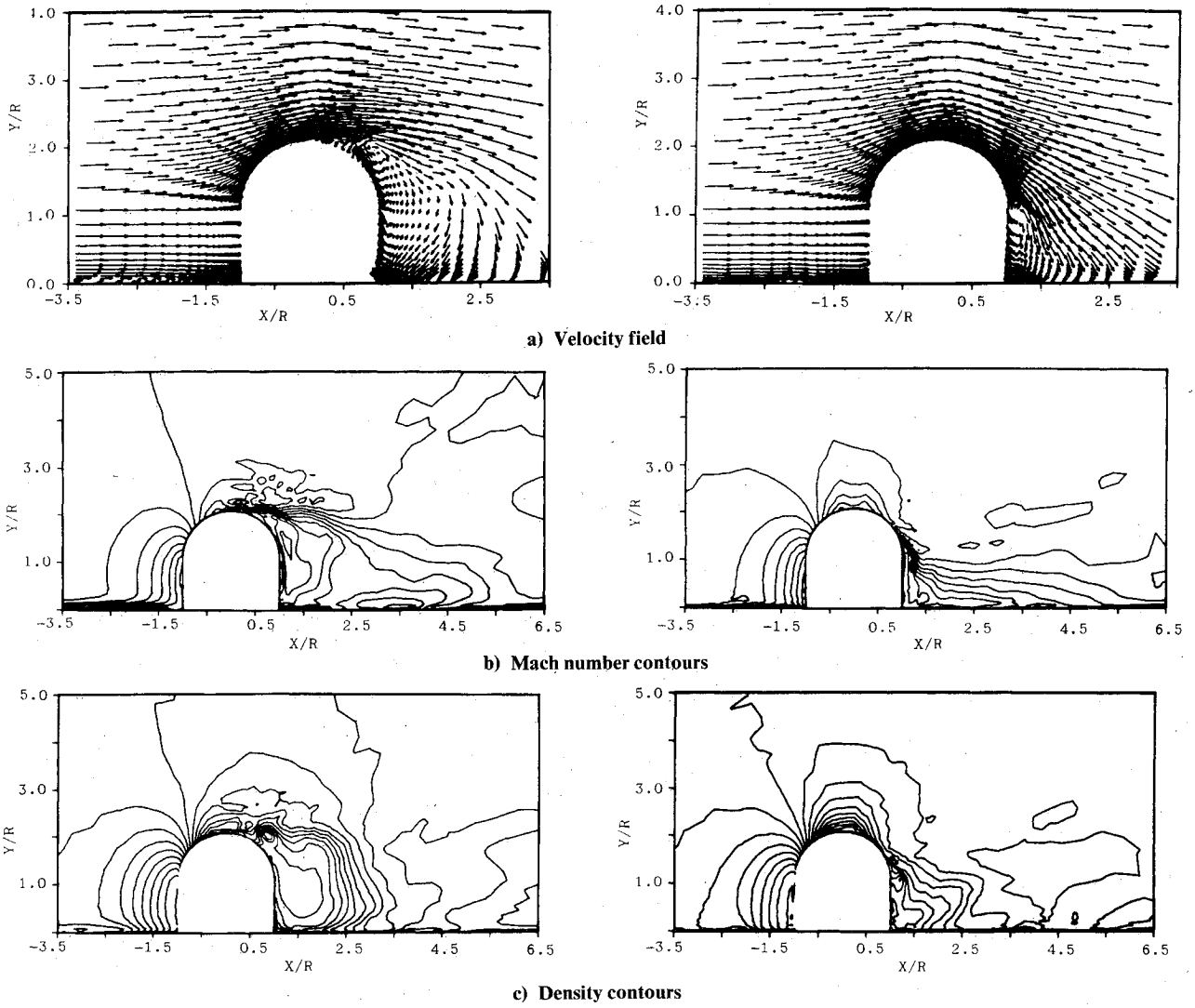

Fig. 9 Flowfield structure in the cross-sectional plane.

N' = (number of half nodes) = 1, S = (number of saddle points) = 4, S' = (number of half saddle points) = 5.

These numbers satisfy the following topological rule for streamliners on a two-dimensional plane cutting the three-dimensional body:

$$(\Sigma_N + \tfrac{1}{2}\Sigma_{N'} - (\Sigma_S + \tfrac{1}{2}\Sigma_{S'}) = -1 \qquad (19)$$

The asymmetry in the flow is further exemplified in Fig. 7 showing the local Mach number distribution for the azimuth angle of 90 deg (cut-out side) and 270 deg (smooth side). Close to the flat plate (Fig. 7a), the cut-out side records lower Mach number. The recovery is only 77% of the freestream value at the outer boundary which is less than 5% of its value at the smooth side outer boundary. This may be associated with the strong vortical flow near the rear edge of turret window and the dominant viscous effects. A significant difference is observed at the turret shoulder (Fig. 7b), where the Mach number attains its peak values 0.83 and 0.62 very close to the body, and asymptotically approaches the freestream value within 1.5 turret radii. The experimental data[15,16] also endorse these values.

In Fig. 8, we present the rms density fluctuations, normalized by freestream density for the azimuth angle 90 deg. Each curve represents the density fluctuations, at a fixed turret height, along a normal direction. The peak value, 0.0405, happens to be at the turret window base. As we move upward this peak value shows a decreasing trend and then oscillates between 0.009 and 0.003. The corresponding peak value[11] (experimental) is 0.034. This experimental value was deduced from the hot-wire data using an empirical relation and ignoring the higher order pressure fluctuations. The far-field fluctuations, which are small, might not be of major concern, but in the near field the turret base is most sensitive to such fluctuations.[17]

Figure 9 gives a glimpse of the flowfield structure in the cross-sectional plane (azimuth angle 0-180 deg) of the computational domain. It presents the instantaneous velocity field, Mach number, and density contours. The significant upstream influence is confined close to the flat plate up to 2.5 times the turret radius. The velocity field is suggestive of an interesting feature that along the front stagnation line on the cylindrical surface, the flow is almost divided into two parts. At $Y/R = 0.3543$, the magnitude of the axial velocity component is negligible compared to the tangential and normal components. The accelerating flow at the hemispherical dome, with a maximum Mach number of 0.87 at 72 deg MPA upstream is separated at 47 deg MPA in the downstream direction. The reverse flow in the near wake region and at the turret shoulder and their time-dependent variation provide the mechanism for vortex shedding and the relative movement of reattachment point.

Complementary to this cross-sectional plane, the flowfield distribution in the plane parallel to the flat plate offers a qualitative comparison to flow past a cylinder. In this plane, up to the turret shoulder, the fluid phenomenon shows a

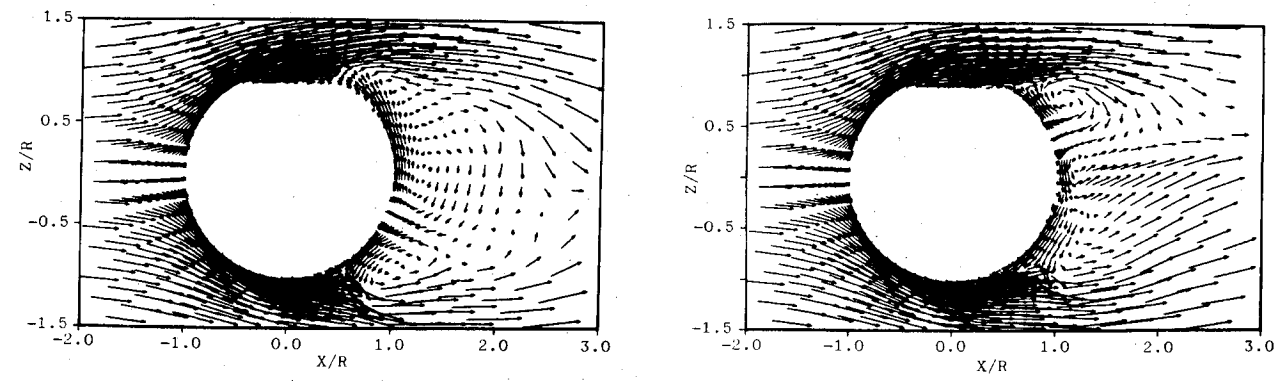

a) Velocity field

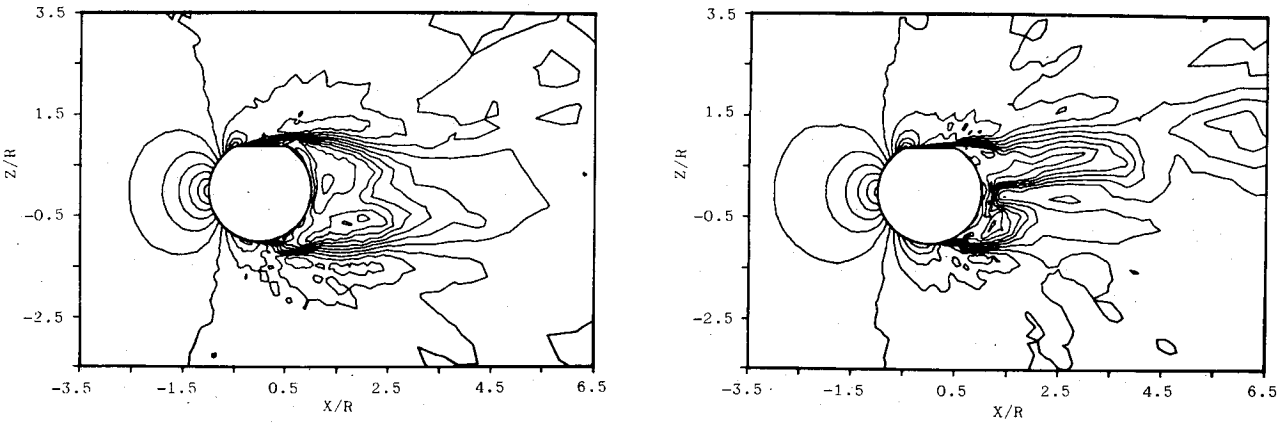

b) Mach number contours

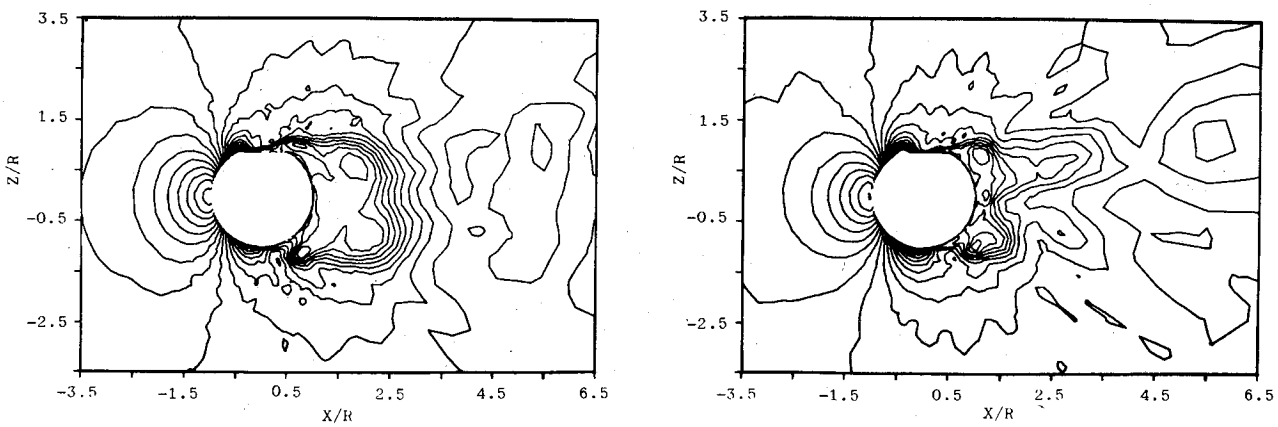

c) Density contours

Fig. 10 Flowfield structure around the turret shoulder.

similar trend. As a typical example, the velocity field distribution, Mach number, and density contours are presented in Fig. 10. The turret window contributes an additional amplification to the process of vortex shedding in the downstream direction. The maximum local Mach number attained was 0.93 at AZA = 63 deg and 0.90 at AZA = 270 deg. These values are much lower than that for the corresponding two-dimensional case,[10] where transition and even shock wave formation is reported. Also, the separation point has advanced further downstream, toward the rear stagnation pont at AZA = 99 and 243 deg, respectively. Even though the separation point location is a function of time, it is observed that for a particular instant of time, the locus of the separation point, the separation line, changes its course considerably along the turret height. This illuminating fact is further revealed in Fig. 11.

This figure shows an instantaneous limiting streamline pattern of the turret surface. Identifying the singular points (Fig. 12) and regrouping them, we get $N=3$, $S=3$. The singular points at the turret base are no more "half," as they are complemented by the corresponding points on the flat surface. Thus, we get another confirmation to the topological criteria. For the skin friction lines on a three-dimensional body B, connected simply to a plane wall P, the sum of nodes, Σ_N and the sum of saddle points, Σ_S satisfy the following relation[6]

$$(\Sigma_N - \Sigma_S)_{P+B} = 0 \tag{20}$$

The asymmetric separation lines start just above the focuses, at the turret base, climb up toward the hemisphere, and then meet at the rear stagnation line at 30 deg MPA. The separation effects on the turret top are mostly confined to 63 deg MPA. On the cylindrical surface, near the turret shoulder, the separation points show a tendency to move upstream indicating that strong three-dimensional flow exists. The asymmetry in the separation line is very much induced by

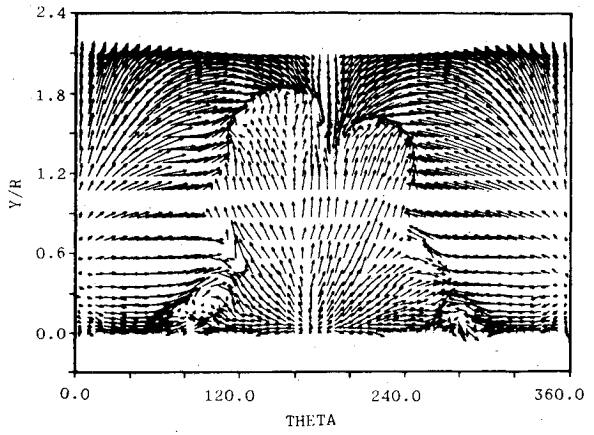

Fig. 11 Instantaneous limiting streamline pattern on the turret surface.

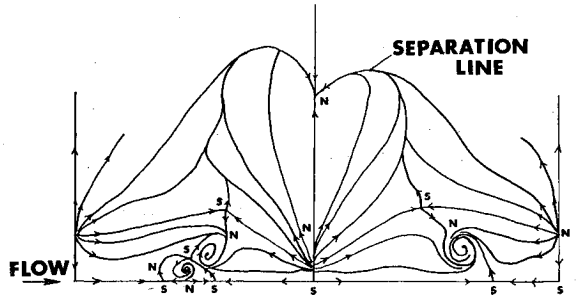

Fig. 12 Interpretation of the skin-friction lines on the turret surface.

the presence of the additional foci and the cut-out in the turr geometry.

Conclusions

An efficient numerical procedure is accomplished successfully for the three-dimensional separated flow around a turret. An adequate description of flow structure is obtained and an endorsement of a topological criterion is presented. For a freestream Mach number of 0.55 and a Reynolds number of 10.3×10^6/m, good comparison is established between our computed results and the experimental data for both the pressure distribution and levels of rms density fluctuations.

Acknowledgments

The authors acknowledge the support provided by Lt. Col. John J. Russell and Capt. Richard K. deJonckheere of the Air Force Weapons Laboratory at Kirtland for the use of the CRAY-1 computer through our exchange program.

References

[1] Sedney, R. and Kitchens, C. W., "The Structure of Three-Dimensional Separated Flow in Obstacle, Boundary Layer Interaction," AGARD-CP-168, Dec. 1975.

[2] Westkaemper, J. C., "Turbulent Boundary Layer Separation Ahead of a Cylinder," *AIAA Journal*, Vol. 6, July 1968, pp.1352-1355.

[3] Farivar, Dj., "Turbulent Uniform Flow Around Cylinder of Finite Length," *AIAA Journal*, Vol. 19, March 1981, pp. 275-281.

[4] Korkegi, R. H., "Survey of Viscous Interactions Associated with High Mach Number Flight," *AIAA Journal*, Vol. 9, May 1971, pp. 771-784.

[5] Dolling, D. S. and Bogdonoff, S. M., "Scaling of Interactions of Cylinders with Supersonic Turbulent Boundary Layer," *AIAA Journal*, Vol. 19, May 1981, pp. 655-657.

[6] Peake, D. J. and Tobak, M., "Topology of Two-Dimensional and Three-Dimensional Separated Flows," AIAA Paper 79-1480, Williamsburg, Va., July 1979.

[7] Hunt, J. C. R., Abell, C. J., and Peterka, J. A., "Kinematical Studies of the Flow Around Free or Surface Mounted Obstacle; Applying Topology to Flow Visualization," *Journal of Fluid Mechanics*, Vol. 86, Pt. 1, 1978, pp. 179-200.

[8] Wang, K. C., "Separation of Three-Dimensional Flow," Rept.. MML TR-76-55C, Martin Marietta Laboratories, Aug. 1976.

[9] Maskell, E. C., "Flow Separation in Three-Dimensions," RAE Aero Rept. 2565, Nov. 1955.

[10] Shang, J. S., "Oscillatory Compressible Flow Around a Cylinder," AIAA Paper 82-0098, Orlando, Fla., Jan. 1982.

[11] DeJonckheere, R. K., Russell, J. J., and Chou, D. C., "High Subsonic Flow Field Measurements and Turbulent Flow Analysis Around a Turret Protuberance," AIAA Paper 82-0057, Orlando, Fla., Jan. 1982.

[12] Shang, J. S., Bunning, P. G., Hankey, W. L., and Writh, M. C., "Performance of a Vectorized Three-Dimensional Navier-Stokes Code on a CRAY-1 Computer," *AIAA Journal*, Vol. 18, Sept. 1980, pp. 1073-1079.

[13] Shang, J. S., "Numerical Simulation of Wing-Fuselage Interference," AIAA Paper 81-0048, St. Louis, Mo., Jan. 1981.

[14] MacCormack, R. W., "The Effect of Viscosity in Hypervelocity Impact Cratering," AIAA Paper 69-354, Cincinnati, Ohio, April-May 1969.

[15] Rose, W. C., "Measurement of Aerodynamic Parameters Affecting Optical Performance," AFWL-TR-78-191, March 1979.

[16] Rose, W. C., Craig, J. E., and Raman, K. R., "Nearfield Aerodynamic and Optical Propagation Characteristics of a Large Scale Turret Model," AFWL-TR-81-28, Air Force Weapons Laboratory, Air Force Systems Comman, Kirtland AFB, New Mex, Nov. 1981.

[17] Purohit, S. C., "Numerical Simulation of Flow Around a Three-Dimensional Turret," AFWAL-TR-82-3075, Nov. 1982.